This document is confidential and is proprietary to the American Chemical Society and its authors. Do not copy or disclose without written permission. If you have received this item in error, notify the sender and delete all copies.

Surface roughened graphene oxide microfibers enhance electrochemical reversibility

Journal:	*Langmuir*
Manuscript ID	la-2024-010042.R1
Manuscript Type:	Article
Date Submitted by the Author:	14-May-2024
Complete List of Authors:	Ostertag, Blaise; University of Cincinnati, Chemistry Porshinsky , Evan; University of Cincinnati, Chemistry Nawarathne, Chaminda; University of Cincinnati Ross, Ashley; University of Cincinnati, Chemistry

SCHOLARONE™
Manuscripts

Surface roughened graphene oxide microfibers enhance electrochemical reversibility

Blaise J. Ostertag,[1] Evan J. Porshinsky,[1] Chaminda P. Nawarathne,[1] and Ashley E. Ross[1,*]

[1]University of Cincinnati
Department of Chemistry
312 College Dr.
404 Crosley Tower
Cincinnati, OH 45221-0172, USA

Office Phone #: 513-556-9314
Email: Ashley.ross@uc.edu

*Corresponding author

ORCID

Blaise J. Ostertag 0000-0003-4970-9742

Ashley E. Ross 0000-0003-2456-3636

Chaminda P. Nawarathne 0000-0003-4760-463X

Keywords: graphene oxide, electrochemistry, sensors, voltammetry, surface roughness

Abstract

Here, we provide an optimized method for fabricating surface roughened graphene oxide disk microelectrodes (GFMEs) with enhanced defect density to generate a more suitable electrode surface for dopamine detection with fast-scan cyclic voltammetry (FSCV). FSCV detection, which is often influenced by adsorption-based surface interactions, is commonly impacted by the chemical and geometric structure of the electrode's surface, and graphene oxide is a tunable carbon-based nanomaterial capable of enhancing these two key characteristics. Synthesized GFMEs possess exquisite electronic and mechanical properties. We have optimized an applied inert argon (Ar) plasma treatment to increase defect density, with minimal changes in chemical functionality, for enhanced surface crevices to momentarily trap dopamine during detection. Optimal Ar plasma treatment (100 sccm 60 s 100 W) generates crevice depths of 33.4 $\pm$ 2.3 nm with high edge plane character enhancing dopamine interfacial interactions. Increases in GFME surface roughness improve electron transfer rates and limit diffusional rates out of the crevices to create nearly reversible dopamine electrochemical redox interactions. The utility of surface roughened disk GFMEs provide comparable detection sensitivities to traditional cylindrical carbon fiber microelectrodes while improving temporal resolution ten-fold with amplified oxidation current due to dopamine cyclization. Overall, surface roughened GFMEs enable improved adsorption interactions, momentary trapping, and current amplification expanding the utility of GO microelectrodes for FSCV detection.

Introduction

Here, we synthesized roughened, surface defect-enhanced graphene oxide (GO) microfibers for ultrasensitive, electrocatalytically enhanced, subsecond neurochemical detection. Fast-scan cyclic voltammetry (FSCV) at carbon fiber (CF) microelectrodes (CFMEs) is one of the most prominent electroanalytical tools for measuring real-time neurochemical signaling.[1–3] CFMEs enable low limits of detection with a large working potential window permitting rapid neurochemical detection in biological samples.[1,4,5] Unfortunately, CF's heterogenous molecular framework[1,6,7] hinders uniform and robust surface manipulation with limited interfacial interactions of numerous neurochemical structural classes resulting in recent work exploring new carbonaceous materials to overcome CFME disadvantages[8–10] and enhance FSCV measurements.[11–17] The tunability of carbon-based substrates is important for improving neurochemical surface interactions[11] resulting in many groups exploring novel carbon nanomaterials to compensate for CFME deficiencies.[11,14–16,18–25] Surface geometry/chemistry improvements provided by materials such as carbon nanotube yarns,[22–24] carbon nanohorns,[26] carbon nanospikes,[19,27] carbon nanofibers,[21] etc. enhance the rapid and sensitive nature of these neurochemical measurements. Graphene-based substrates, derived from nanosheets, are another novel electrode with a tunable 2-dimensional geometry of two well-defined planes: basal and edge.[17,28–30] The conjugated sp^2 hybridized basal plane is atomically flat with low defect density whereas the sp^3 hybridized edge plane consists of high levels of defects and functional groups.[31,32] We previously developed graphene oxide microelectrodes (GFMEs) for neurochemical detection with FSCV.[17] GFME's contain highly oxidized graphene sheets with high specific surface area and electrical conductivity, which lead to significant enhancements in sensitivity, kinetics, fouling resistance, and electrochemical reversibility.[17,30,33] GFMEs have also recently expanded our understanding of specific neurochemical-electrode interactions[17,30]

displaying the attractiveness of the substrate's tunable surface. This work provides a method for increasing GFME surface roughness for stable, ultrasensitive, temporally resolved FSCV detection.

Tunable graphene materials are used commonly for energy storage applications due to their attractive mechanical, thermal, and electronic properties.[34–38] Graphene fiber materials have adopted these properties exhibiting high conductivity and flexibility[33,39–41] which are attractive for FSCV neurochemical detection.[17,30] GO's highly oxidized surface is attractive for electrochemical detection because of its surface defects, hydrophilic properties, and attractive oxygen functionality for cationic neurochemicals.[17,20,30,42,43] The Venton group studied dopamine detection at CFMEs electrodeposited with GO showing enhanced detection sensitivity and limits of detection.[20] The Cui group also generated similar improvements to dopamine detection by fabricating fuzzy graphene microelectrode arrays.[42] Hydrothermal methods, microfluidic assemblies, wetspinning, and ion cross-linking procedures have even permitted the fabrication of individual graphene fibers.[33,44–46] These novel studies inspired our group's recent push for fabricating GFMEs to evaluate specific neurochemical interactions at well-defined carbon surfaces.[17,30] GFMEs not only enhance electron transfer, frequency dependence, and fouling resistance,[17] but recent studies from our lab have fine-tuned GO sheet alignment to show some neurochemicals fail to interact at edge-plane sites, a controversial finding in electrochemistry.[30] These results add to the ongoing conflict of attractive edge vs. basal plane electrochemical properties and inspired us to explore how altering the surface roughness of these novel electrodes impacts neurochemical detection with FSCV.

Here, we provide an optimized method of plasma treating GFMEs for increased surface roughness to enhance dopamine detection with FSCV. The surface topology of GO substrates can be manipulated by various methods to generate enhanced surface roughness[47] or holes in membranes/films;[34–36,40] applications use GO substrate treatments to tune the surface structures for enhanced performance in supercapacitors, CO_2 capture, water distillation, etc., but these

substrates cannot be easily fabricated into microfiber frameworks. We have previously demonstrated that inert plasma treatments with argon (Ar) do not alter CFME surface functionalization but enhance neurochemical adsorption strength, electrochemical reversibility, sensitivity, and electron transfer kinetics.[13] Surface roughness plays an important role in improving adsorption interactions at CFMEs and has shown to promote local trapping phenomena for dopamine with FSCV.[13,14,18,21,22,24] Because of the wealth of knowledge of how geometry impacts dopamine detection with FSCV, we chose to study the impact of surface roughening of GO microfibers on FSCV detection. We adapted and modified our previously published method for Ar-plasma treated CF to investigate the extent to which Ar-plasma influences electrochemical detection at GFME's. Overall, we observed a two-fold increase in surface roughness following optimal Ar plasma treatment. Ar plasma treated GFMEs are highly stable and display enhancements in surface defects permitting highly sensitive, temporally resolved dopamine measurements with FSCV. The microfibers in this work improve the overall performance of GFMEs with slight surface functionality alterations providing an efficient method of evaluating neurochemical interactions at roughened, defect-dense GO surfaces.

Experimental Methods

Reagents

GO microfibers were synthesized from a mixture of a single-layer GO dispersion in water (10 mg mL^{-1}) purchased from ACS Material (Pasadena, CA, USA) and L-ascorbic acid (99%) purchased from Sigma Aldrich (St. Louis, MO, USA). GO microfiber chemical additives include potassium hydroxide (≥ 99.98%) purchased from Thermo Fisher Scientific (Waltham, MA, USA) and sodium hydroxide (≥ 97.0%), polyacrylonitrile (or PAN, MW = 150,000), poly(methyl methacrylate) (or PMMA, MW = 350,000), and poly(3.4-ethylenedioxythiopene)-poly(styrenesulfonate), 3.0-4.0% in H_2O (or PEDOT:PSS) purchased from Sigma Aldrich. Tris

buffer is prepared in Milli-Q deionized water (Millipore, Billerica, MA, USA) consisting of 15 mM Tris Base, 140 mM NaCl, 3.25 mM KCl, 1.25 mM NaH_2PO_4 monohydrate, 1.20 mM $MgCl_2$ hexahydrate, 2 mM Na_2SO_4 anhydrous, and 1.20 mM $CaCl_2$ dihydrate all purchased from Thermo Fisher Scientific. The chemical reagents HCl and dopamine were purchased from Thermo Fisher Scientific while serotonin hydrochloride was purchased from Sigma Aldrich. 10 mM dopamine stock solutions were stored at 4°C after dissolving in 0.1 M HCl. Tris buffer (pH = 7.40) was used to dilute stock solutions to derive experimental solutions.

Graphene oxide microfiber synthesis

A modified hydrothermal method was used to synthesize randomly aligned GO nanosheets / misaligned GO microfibers similar to our previously published work.[17,30] In summary, a 10 mg mL^{-1} dispersion of GO in water was combined with 1% w/w L-ascorbic acid (AA) and stirred to ensure solution homogeneity. The GO-AA solution was then placed in a 3 mL transfer pipet (Globe Scientific, Inc., Mahwah, NJ, USA) coupled with a 10 μL micropipette tip (Mettler-Toledo, LLC, Columbus, OH, USA) and injected into a glass capillary tube (1 mm x 0.25 mm; A&M Systems, Inc., Sequium, WA, USA). Capillary tubes were then sealed using air-dry epoxy (J-B Weld 50112 ClearWeld Quick Setting Epoxy Syringe – Clear) and placed at 80 °C for 24 h. After setting, the epoxy seal was removed, and capillaries remained in the oven for 24 h for complete dryness and fiber formation. Finally, capillaries were placed in isopropyl alcohol for 20 min and the fibers were extracted.

Graphene oxide microelectrode fabrication

GO disk microelectrodes were constructed similar to prior reports.[17,30] Shortly, GO fibers were vacuum aspirated into glass capillary tubes (1.2 mm x 0.68 mm, A-M Systems, Inc., Sequium, WA, USA) and pulled using a vertical Narishige PE-22 electrode puller (Tokyo, Japan). GO fibers were cut to the glass seal and sealed using Epoxy Resin 828 and 14% w/w 1,3-phenylenediamine heated at 80 °C. The electrodes were then submerged for 3 s in acetone to

remove excess epoxy and cured at 110 °C for 12 h. Electrodes were polished at 45 ° for 30 min using a diamond abrasive plate to produce a polished disk microelectrode. Acquisition of electrochemical data was preceded with soaking electrodes in isopropyl alcohol for 10 min and backfilling with 1 M KCl.

Graphene oxide microelectrode plasma surface treatment

GO disk electrodes were plasma treated using a CS-1701 RIE plasma etcher (Nordson MARCH, Westlake, OH, USA) with a 13.56 MHz RF generator. The electrodes were placed inside the plasma etcher and Ar plasma was delivered at a constant pressure of 70 torr, flow rate of 100 sccm (standard cubic centimeters per minute), and a varied plasma application time and power. Plasma treatment time and power were optimized using a combination of scanning electron microscopy (SEM) imaging for fiber deterioration information and electrochemical detection analyzing electrochemical reversibility of dopamine's redox mechanism.

Material characterization

Standard surface characterization techniques were used to analyze the physical and chemical properties of untreated and Ar-treated GO microfibers/microelectrodes. SEM micrographs qualitatively assessed individual fibers and disk electrodes using an FEI XL30 SEM (Advanced Materials Characterization Center, University of Cincinnati, Cincinnati, OH, USA). Atomic force microscopy (AFM) imaging quantitatively analyzed surface roughness of the side/profile of individual untreated and Ar-treated GO microfibers. AFM images were acquired in non-contact tapping mode at a frequency of 1 Hz and 512 x 512-pixel resolution (Bruker Dimension Icon ScanAsyst AFM, Billerica, MA, USA). Raman spectroscopy was performed on polished disk electrodes using a Renishaw *InVia* Reflex spectrometer (Guocestershire, UK) controlled by WiREInterface excited by a 633 nm Ar-ion laser at 10% power and an integration time of 10 s to acquire 7 μm x 7 μm Raman maps. X-ray photoelectron spectroscopy (XPS) analyzed elemental composition of GO fiber surfaces before and after Ar plasma treatment using

a ThermoScientific Nexsa X-ray Photoelectron Spectrometer with a hemispherical analyzer and monochromatic Al Kα source (Wayne State University, Detroit, MI, USA). Samples were mounted using conductive Cu tape and a base pressure of 1.7 x 10^{-7} mbar was used for data acquisition with a flood gun employed for surface charge neutralization.

Electrochemical detection methods

Cyclic voltammetry was performed using a CH Instruments electrochemical workstation (Model 620, Bee Cave, TX, USA). A single component electrochemical cell was used in a three-electrode configuration with a GO working microelectrode, Pt wire counter electrode, and Ag/AgCl (3 M KCl) reference electrode. Fast-scan cyclic voltammograms were collected using a WaveNeuro potentiostat (Pine Instruments, Durham, NC, USA). Reported cyclic voltammograms were background subtracted to remove non-faradaic current as the electrode was scanned using dopamine's traditional waveform (scanning at 400 V s^{-1} from -0.4 V to 1.3 V and back at a repetition rate of 10 Hz). The working electrode was equilibrated for 10 min prior to data acquisition and the average current, from three consecutive injections, for each analyte was recorded. All electrodes were tested in a home-built flow injection setup consisting of a six-port HPLC actuator (Valco Instruments, Houston, TX, USA) and syringe pump (Model Fusion 100, Chemyx, Stafford, TX, USA) set to a constant flow rate of 1 mL min^{-1} to deliver buffer. All experiments were performed at room temperature.

Statistics/Graphics

GraphPad Prism V. 10.0 (GraphPad Software Inc., La Jolla, CA, USA) software was used to create graphical depictions and perform statistics. Data was reported statistically significant with statistical p-values at a 95% confidence interval ($p < 0.05$). All values are reported as mean ± standard error of the mean with electrode number denoted by *n*. Raman spectroscopy data was analyzed in Wire 5.5 (Renishaw, Wotton-under-Edge, United Kingdom), and Raman spectroscopy and XPS graphs were plotted using Origin Pro 2022.

Results and Discussion:

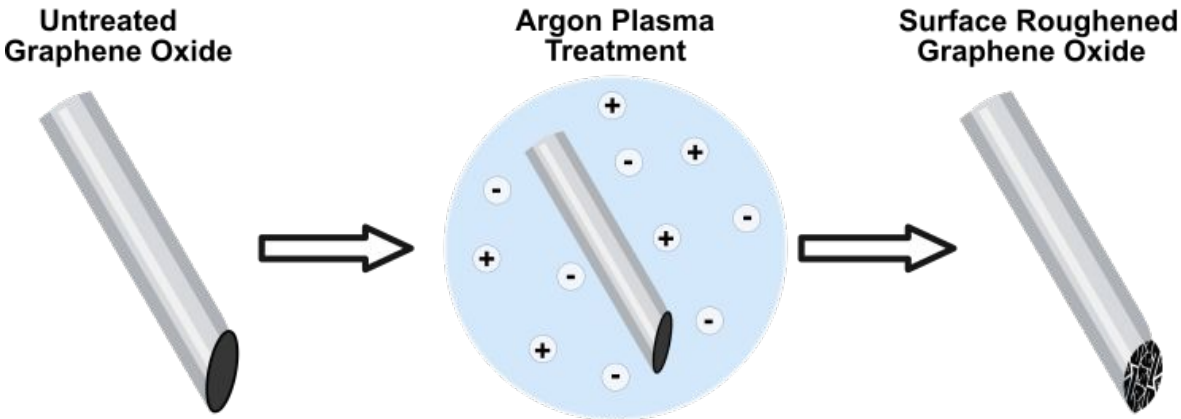

Figure 1. Schematic of the fabrication process of surface-roughened GO microfibers using Ar plasma for improved dopamine interfacial interactions and electrochemical reversibility. Disk GO microelectrodes are treated with Ar plasma to form a roughened electrode surface with no added functionalization (created in Biorender.com)

Surface-roughened graphene oxide microfiber fabrication and characterization

GFMEs were fabricated following a modified hydrothermal procedure[17,30,48,49] to fabricate microfibers of 24.9 ± 1.2 μm in diameter (n = 6). By facilitating enhanced π-π interactions between GO sheets, the modified hydrothermal procedure with the addition of 1% w/w L-ascorbic acid allows for mild heating conditions to promote 3D GO sheet microfiber framework formations. Microfibers were aspirated through a glass capillary and vertically pulled electrodes were epoxy sealed and polished to produce a 45 ° micro-disk electrode (Figure 1). Hand-fabrication creates slight deviations in electrode surface area, but batch-to-batch fiber diameters are reproducible with consistent electrochemical performance prior to surface roughness treatments. Surface roughness and defects have been shown to impact electrochemical performance enhancing electron transfer rates with increased edge plane character.[6,7,13,30] To generate increased surface roughness and disorder degrees, various GO dispersion chemical additives and microfiber

treatments were evaluated electrochemically to determine the optimal method for reproducible surface roughened GFMEs (Figure S1).

Many reports use surface treatments and/or chemical additives for surface morphology alterations of GO substrates to enhance porosity and surface roughness.[34–36,40,47] Here, we elected to adopt several of these methods in an effort to generate optimal GFME surface roughness for FSCV detection of dopamine. Chemical additives explored in this manuscript include activation agents like potassium hydroxide and sodium hydroxide or polymers like PEDOT:PSS, PMMA, or PAN (Figure S1); for information on the synthetic processes used for GO microfiber formation with these chemical additives, see Supporting Methods. These chemical additives were either mixed into GO dispersions for fiber formation or used to soak GO microfibers after formation. Heat treatment procedures followed to induce kinetically driven activation of the GO microfibers or to degrade polymer additives. Surface roughness methods were not further investigated if they resulted in poor electrochemical performance, poor fiber mechanical properties, or irreproducible fabrication of fiber frameworks (See Figure S1 for example SEM images of some GO microfibers fabricated). Additives like 10% w/w PEDOT:PSS heated to 390°C for 30 mins (Figure S1 C) or soaking GO microfibers in 7 M KOH (Figure S1F) resulted in negligible improvements in GFME electrochemical performance following treatment conditions with no evidence of enhanced dopamine interfacial interactions. Meanwhile, additives like 10% PEDOT:PSS heated to 250°C for 15 mins or 45 mins (Figures S1 B&D) or 1:3 KOH:GO heated to 800°C for 60 min exhibit non-circular GO microfiber cross-sections and non-uniform microfiber frameworks which can also cause poor microfiber mechanical properties. Many of these procedures also involve thermal treatments capable of reducing GO, which ultimately alters the chemical structure of the GFMEs. Overall, the results from these tests led to exploring plasma surface treatments to roughen the GFME surface. Ar plasma is capable of physically etching carbon by bombarding the surface with Ar+ ions without introducing surface chemical reactions

making it a viable surface treatment for accomplishing morphological changes to GFME surface roughness. The deteriorated frameworks or inadequate electrochemical performance for several of the approaches discussed above resulted in Ar plasma being deemed the optimal surface roughening method due to its inert nature and ability to use regularly synthesized GO microfibers without causing detrimental changes to the fiber integrity (Figure 1). Additionally, electrochemical characterization revealed evidence of enhanced electrochemical performance of Ar plasma treated GFMEs. All information in the following sections pertains to Ar-plasma treated GO fibers.

Surface Characterization – Morphological Analysis

Scanning Electron Microscopy (SEM). SEM imaging was used to qualitatively assess the surface topology of GFMEs cross-sections before and after Ar plasma treatment (Figure 2). Untreated GFMEs (Figure 2A/B) illustrate a relatively homogenous surface with consistent striations produced by polishing during disk electrode fabrication capable of generating reproducible electrochemical results as discussed in the following sections. Here, the fiber fabrication process matches that of prior reports[17,30] for "misaligned" GO microfibers with randomly assorted GO sheets and were quantitively analyzed electrochemically to determine non-optimal and optimal Ar plasma treatment conditions. Although the impact of Ar plasma on GFME surface roughness is not visually apparent, non-optimal 60 s 90 W treatment (Figure 2C/D) produces increases in noticeable voids adding to the striations present in the untreated GFME (Figure 2A/B). When analyzing 60 s 100 W Ar-treated GFMEs, though, we begin to see the accumulation of voids in the surface accompanied by further increases in striation depth formed from polishing (Figure 2E/F). SEM provides a visual assessment of the surface morphology of untreated and Ar-treated GFMEs showing noticeable increases in surface roughness, but additional surface characterization techniques were used to quantitate the extent these treatments have on GFME surface roughness.

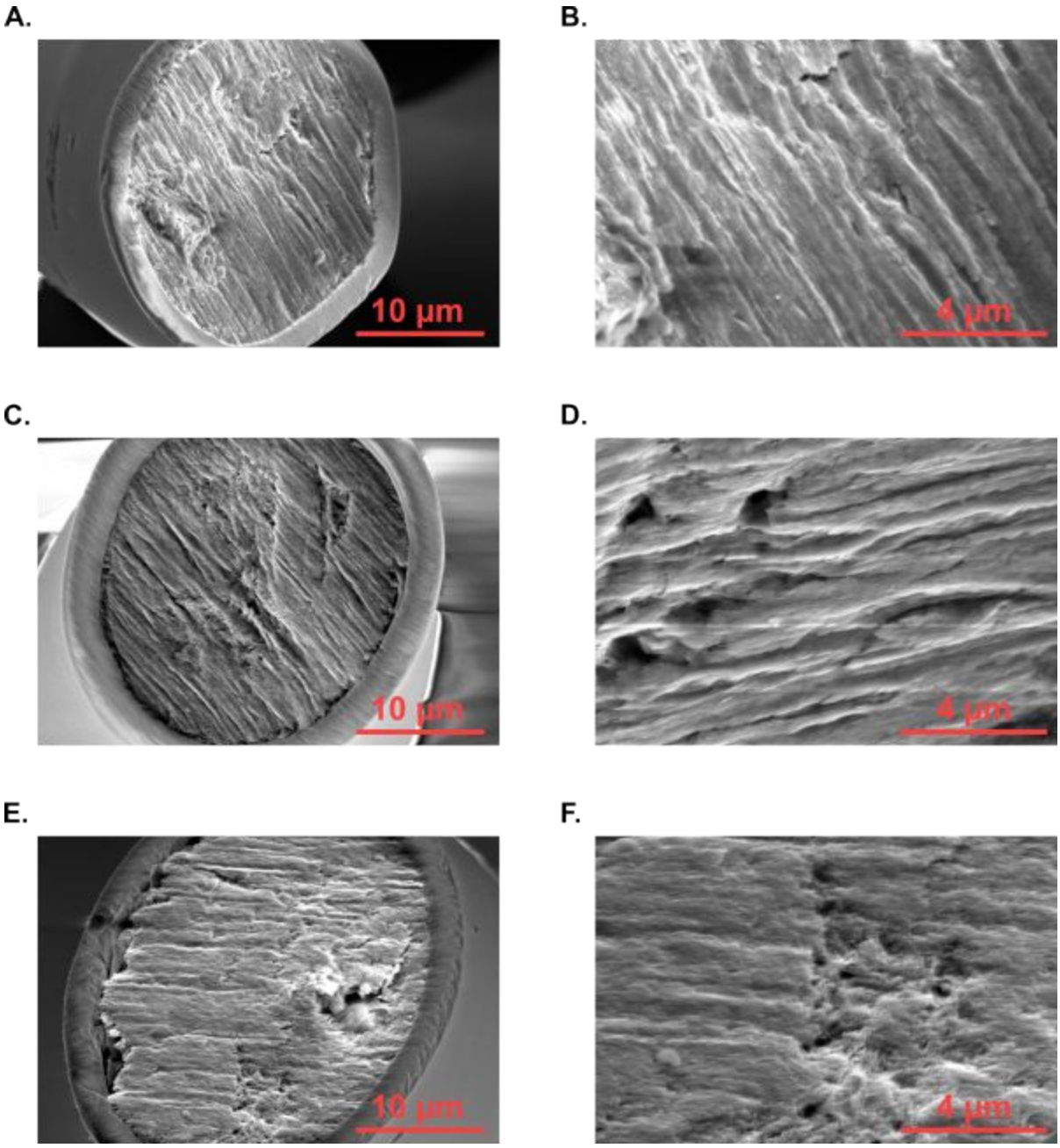

Figure 2: Surface characterization using SEM shows GO microelectrode increased surface roughness following Ar plasma treatment for enhanced analyte-electrode interactions. Ar plasma treatment of GO microelectrodes was optimized using 100 W Ar plasma at a flow rate of 100 sccm. (A/B) Untreated GO. (C/D) GO treated with 90 W Ar plasma for 60 s. (E/F) GO treated with 100 W Ar plasma for 60 s.

Atomic Force Microscopy (AFM). AFM was used to quantitatively evaluate the impact Ar plasma treatment had on the average surface roughness depth (R_z) of GO microfibers. Due to how AFM data is collected, we were only able to measure the longitudinal sides of the fiber, and

not the cross-sections. Depth analysis was performed laterally over a 1 μm x 1 μm area over the side of untreated and 100 W 60 s Ar-treated (electrochemically optimized) GO microfibers with three horizontal cross-sections were used to calculate average surface roughness depth (Figure S2). Qualitatively, AFM images show notable striations on both fiber groups as was observed with SEM, but AFM images also show the accumulation of GO sheets forming well-defined surface structures unseen with SEM (Figure 3). The surface roughness R_z value increases from 15.2 ± 1.0 nm for untreated GO microfibers (Figure 3A) to 33.4 ± 2.3 nm for 60 s 100 W Ar-treated GO microfibers (Figure 3B / Table 1, unpaired t test, $p < 0.0001$, $n = 4$). Cross-sectional insets for untreated GO microfibers (Figure 3A, red) and 60 s 100 W Ar-treated GO microfibers (Figure 3B, blue) show minimal surface roughness deviations in untreated GO microfiber topology compared to Ar-treated GO microfibers. Although surface roughness magnitude is relatively low, we show enhanced surface roughness depth for both untreated and Ar-treated GO microfibers compared to values previously reported for CF, the material of choice for traditional FSCV detection.[14,24] These results show the impact Ar plasma treatment has on GO microfiber surface topology. We hypothesized that the increased surface roughness generated by Ar treatment would facilitate improved neurochemical interactions kinetically and electrochemically, similar to prior reports.[13,14,22,23,27] We note no further AFM characterization was performed (Table 1) on other Ar-treated GO microfibers due to non-optimal electrochemical performance or GO fiber framework deterioration (described in later sections). Average R_z values were reproducible for untreated and Ar-treated GO microfibers, indicating the robustness of the fiber formation method and the plasma treatment .

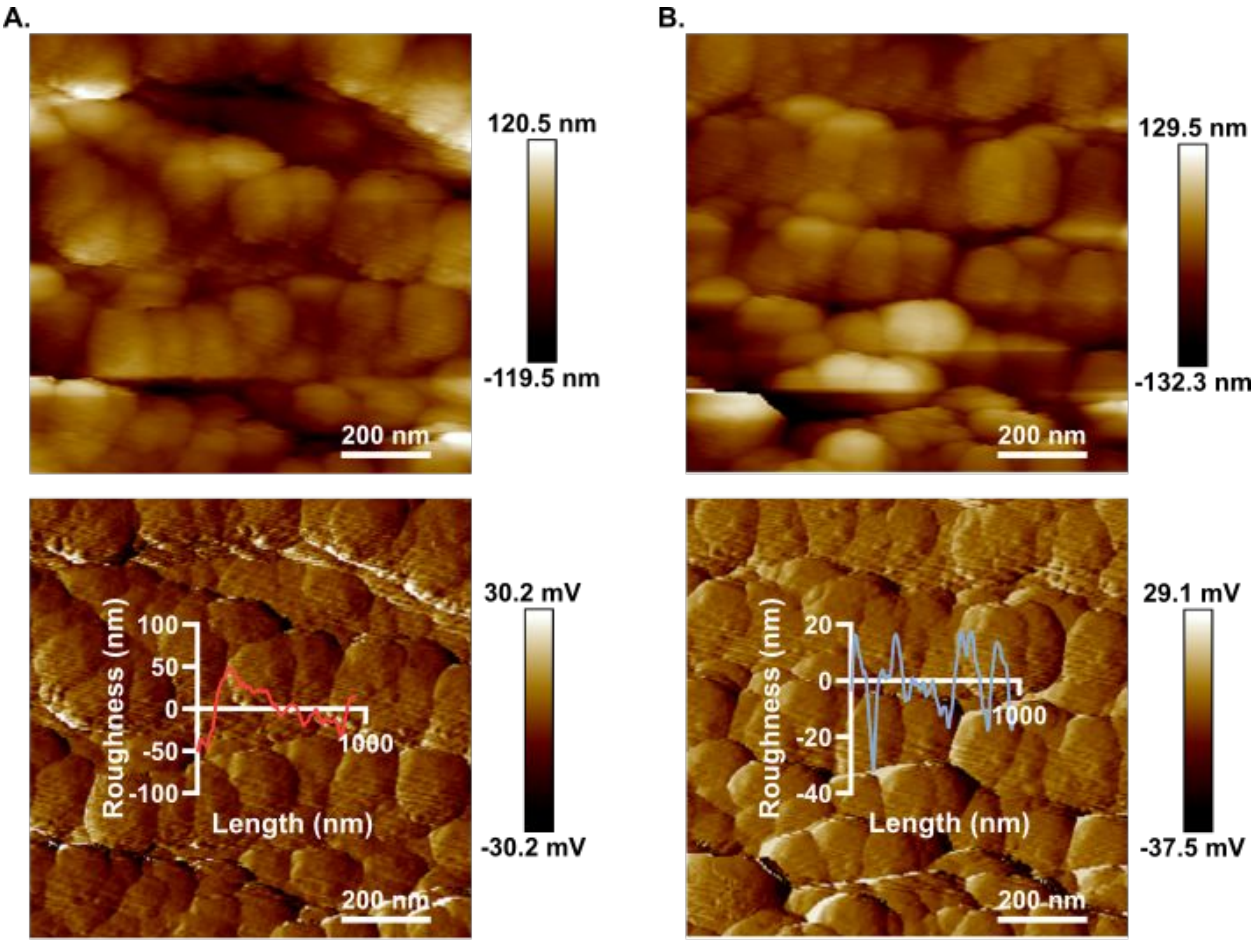

Figure 3. AFM analysis of GO microfibers supports an increase in surface roughness following 100 W Ar plasma treatment compared to untreated GO microfibers. Images were acquired over a 1.0 μm x 1.0 μm area on the profile of the GO microfibers. (A) Untreated GO microfibers exhibit low surface roughness depth (15.2 ± 1.0 nm) with small fluctuations in surface roughness when analyzed horizontally across the image (n = 4; top – height sensor image, bottom – amplitude sensor image with horizontal line scan inserts). (B) 100 W Ar-treated GO microfibers exhibit increased surface roughness depth (33.4 ± 2.3 nm) with large fluctuations in surface roughness when analyzed horizontally across the image (n = 4; top – height sensor image, bottom – amplitude sensor image with horizontal line scan inserts).

Surface Characterization – Disorder Degree and Elemental Analysis

Raman Spectroscopy. Raman spectroscopy can evaluate the microstructure of carbon-based substrates and identify carbon hybridization present across the material's surface. The well-defined, biplanar nature of GO sheets is characterized by the sp^3 hybridized, defect dense, functionalized edge plane and the sp^2 hybridized, low defect, atomically flat basal plane.[31,32] The GO microfiber synthetic procedure randomly orients GO sheets within the fiber's framework

exhibiting a heterogenous chemical microstructure across the electrodes surface.[17,30] We hypothesized that by introducing Ar plasma to the GFME's surface to enhance surface roughness will result in increased defect sites and an increased ratio of edge to basal plane to ultimately improve electrochemical detection.[6,7] Raman surface spectral maps (7 μm x 7 μm, 0.3 μm step size) were acquired along the GFME's 45 ° polished surface and normalized to the disorder (D) peak intensity. We then evaluated the D intensity (I_D) and the graphitic peak intensity (I_G), and analyzed their ratio (I_D/I_G) giving insight into the surface defect degree. Representative spectra for untreated and 60 s 100 W Ar-treated GFMEs are reported in Figure S3 where the D and G bands are deconvoluted with five superimposed peaks. Of note, no further Raman characterization was performed (Table 1) on other Ar treatments due to non-optimal electrochemical performance (described in sections below). The sharper, intense D band (~1350 cm^{-1}) is comprised of defects in the graphitic lattice created by breaks in ideal periodicity[50–52] whereas the less intense G band (~1580cm^{-1}) is comprised of sp^2 hybridized carbon atoms. By evaluating the I_D/I_G ratio we can evaluate the defect degree of the GFME and the greater the ratio implies greater edge plane character attractive for electrochemical detection. Before doing so, the superimposed peaks within both bands are fitted for accurate defect degree representation: D*, D', and D". The D* band (1150-1200 cm^{-1}) deconvolutes the D band and is related to the disordered graphitic lattice from sp^2-sp^3 bonds.[53] The D' (~1620cm-1) and broad D" band (1500-1550) deconvolute the G band and are attributed to disorder-induced phonon mode of crystal effects[54] and the correlation of the band and oxygen content,[53] respectively. These five superimposed peaks were then used to peak fit the Raman spectra acquired (Figure S3) showing evident heterogeneity in the microstructure for "misaligned" GO sheet-derived GFMEs (Figure 4).[17,30] Raman spectral maps were then plotted to analyze the defect degree across the defined 7 μm x 7 μm area of the surface for untreated (Figure 4A) and 60 s 100 W Ar-treated GFMEs (Figure 4B). Following our hypothesis, Ar plasma treatment increases the defect degree of GFMEs from 1.618 ± 0.005

(Figure 4C, n = 3) to 1.857 ± 0.003 (Figure 4C, unpaired t-test, $p < 0.0001$, n = 3); compared to previous reports on plasma treated glassy carbon, the increase in edge plane character we observe is likely enabled through a maintenance of oxygen functionality as opposed to materials like hydrogenated glassy carbon.[55] The increase in peak position of the D* band (Figure 4D) and decrease in D" band position (Figure 4E) following treatment indicates decreased oxygen content[53] implying slight reduction of the GO surface, but the extent is negligible (See X-ray Photoelectron Spectroscopy section). Overall, Raman spectroscopy analysis of Ar plasma treated GFMEs illustrates increases in defect sites and edge plane character accompanied by small decreases in surface oxide functionality.

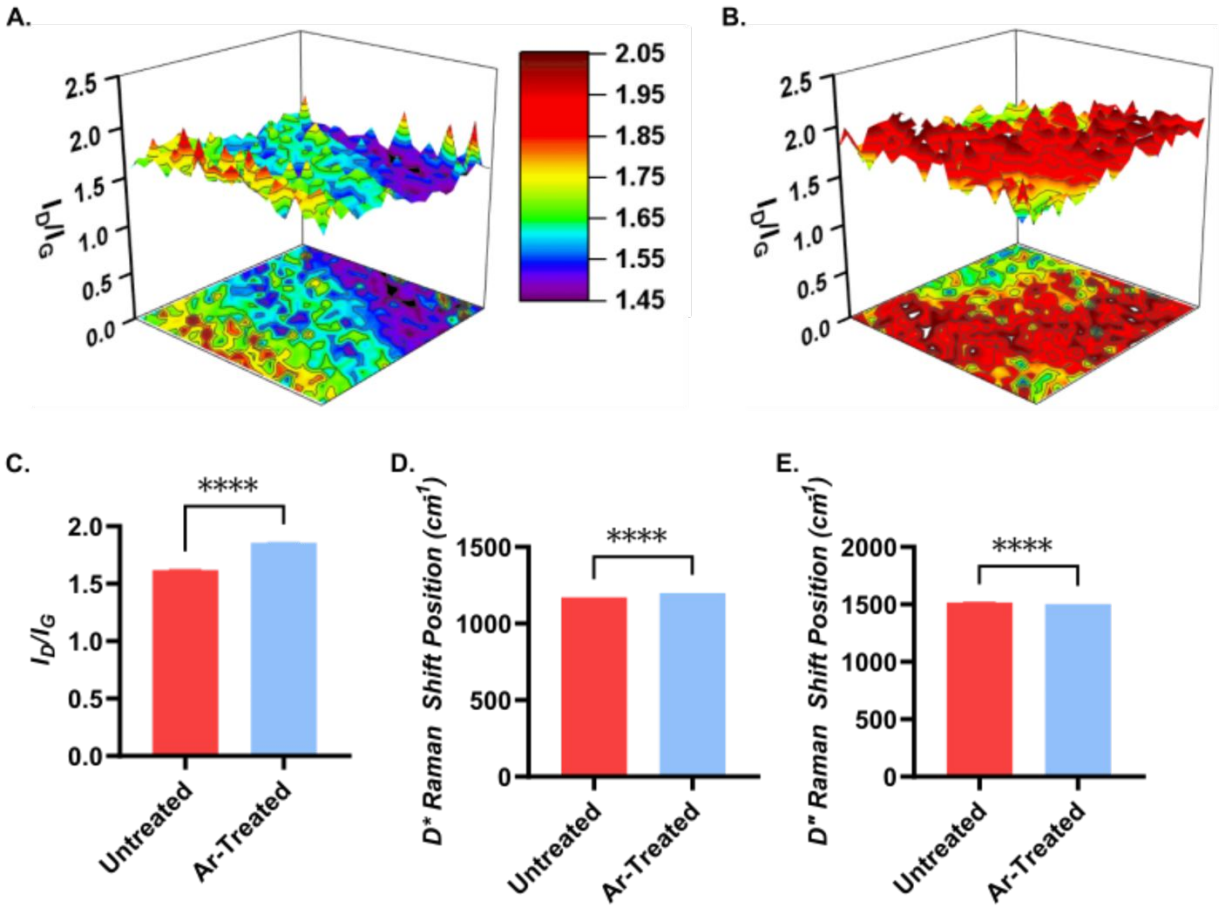

Figure 4. Raman spectroscopy mapping analysis of GO illustrates enhanced defect degrees and higher edge plane character following 100 W Ar plasma treatment with decreased oxygen content. (A) 7 μm x 7 μm, 0.3 μm step size 3-dimensional Raman spectroscopy map of untreated GO (B) 7 μm x 7 μm, 0.3 μm step size 3-dimensional Raman spectroscopy map of 100 W Ar-treated GO. (C) I_D/I_G ratio increases from 1.618 ± 0.005 to 1.857 ± 0.003 following 100 W Ar plasma treatment

(unpaired t-test, $p < 0.0001$, df = 3451, n = 3). (D) D* peak position increases from 1171 ± 0.6 to 1200 ± 0.1 following 100 W Ar plasma treatment (unpaired t-test, $p < 0.0001$, df = 3451, n = 3). (E) D" peak position decreases from 1516 ± 0.4 to 1504 ± 0.1 following 100 W Ar plasma treatment (unpaired t-test, $p < 0.0001$, df = 3451, n = 3).

X-ray Photoelectron Spectroscopy (XPS). GO microfibers were characterized using XPS to provide elemental analysis and ensure Ar plasma treatment does not alter the chemical composition of GO microfibers compared to those untreated (Figure 5). Plasma treatment is a high-powered treatment technique,[13,56–58] so XPS was also used to analyze oxygen composition following treatment as oxide functionality is paramount for adsorption processes of catecholamines when testing these electrodes electrochemically.[4,6,7] Additionally, the fabrication process of GO microfibers uses 1% ascorbic acid (AA), a known reducing agent, to improve GO sheet interactions,[17,30] so the analysis of oxygen composition ensures the microfibers produced are in fact GO. Previous reports have confirmed 1% AA does not impact the surface chemical composition providing evidence that GO microfibers have not been reduced.[17] XPS survey spectra of untreated (red) and 60 s 100 W Ar-treated GO microfibers present two evident peaks for analysis: C 1s and O 1s (Figure 5A). As expected, analysis at a binding energy of ~ 243 eV shows no evident Ar 2p peak confirming no added Ar functionalization to the GO framework (Figure 5B). Upon integration, we show no significant change in the C 1s (77.5% for untreated and 77.7% for Ar-treated GO) and O 1s (22.5% for untreated and 22.3% for Ar-treated GO) weight percentages with negligible oxygen content decreases, similar to the Raman analysis (Figure 5A). Further peak deconvolution of the C 1s and O 1s peaks was required to provide information about the functionality present at untreated and Ar-treated GO surfaces. By fitting these peaks at corresponding binding energies functional groups are identifiable, and we note the presence of five peaks within the C 1s band (Figure 5C) and three peaks within the O 1s band (Figure 5D). Deconvolution of the C 1s band shows an intense graphitic peak centered at 284.7-284.8 eV and C-O peak centered at 285.7 eV for both the untreated (red) and Ar-treated GO microfiber. The

graphitic peak intensity decreases with respect to that of the other four peaks for the Ar-treated GO microfibers. Further deconvolution shows evident changes in functionality as the intensity of the Ar-treated GO microfibers increase respective to the graphitic peak for the three remaining peaks: C-O-C (296.3-286.4 eV), C=O (287.5 eV), and O-C=O (289-289.4 eV). Increases in oxide functionality with respect to the graphitic C 1s peak support Raman spectroscopy analysis showing resultant defect sites and edge plane character increases from increased surface roughness. Interestingly, the increase in oxide functionality we observe is relatively small as to what we expected since plasma treatment generates increased edge plane density prone to more reactive carbon capable of oxidation. We hypothesize these proportionately small increases in the O 1s/C 1s are compensated during the plasma treatment bond breaking process in which voids in the graphene lattice are generated creating reduced graphene oxide structures. This process coupled to increased oxidation at locations where edge plane density is increased results in small changes in this ratio. Relative ratios of the O 1s band do not significantly change following peak fitting analysis aside from a broadened O 1s band for untreated GO microfibers with the presence of the C=O (529.5-530.3 eV), C-O-C (532.3-532.6 eV), and C-O-H (533.5 eV) peaks. These results provide evidence that the improved electrochemical performance discussed in the following sections are not results of changing surface chemical composition but rather due to increasing surface roughness / defect degrees and potentially altering the present surface functional groups.

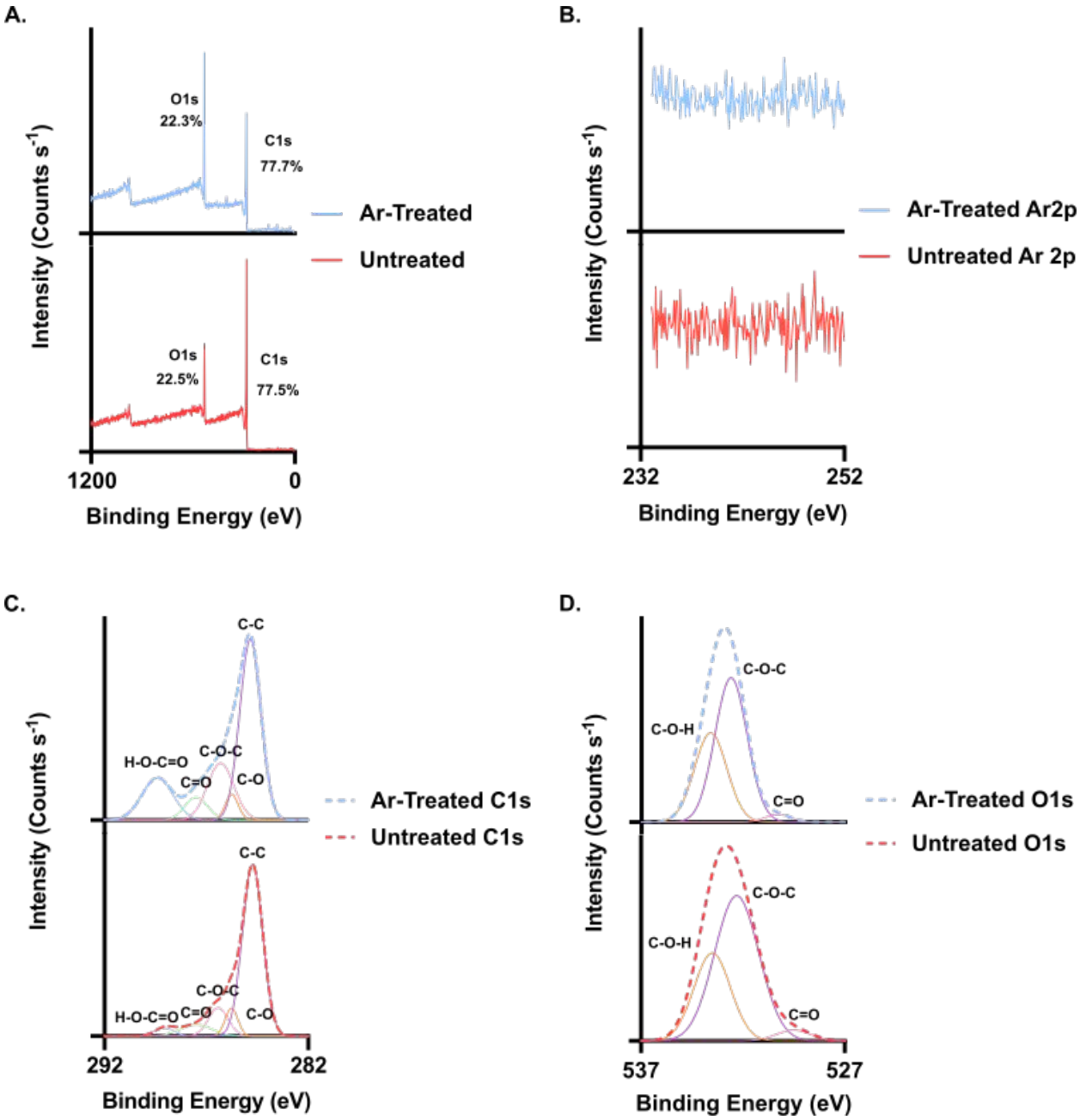

Figure 5. XPS analysis illustrates that Ar plasma treatment of GO microfibers (100 sccm for 60 s) generates no fluctuations in overall surface functionalization and minor fluctuations in specific elemental functionalization. (A) Survey spectra of untreated GO (red, C1s = 77.5%, O1s = 22.5%) and 100 W Ar-treated GO (blue, C1s = 77.7%, O1s = 22.3%). (B) Ar2p raw spectra of untreated GO and 60 s 100 W Ar-treated GO. (C) C1s deconvolution of untreated GO and 60 s 100 W Ar-treated GO**.** (D) O1s deconvolution of untreated GO and 60 s 100 W Ar-treated GO.

Electrochemical Characterization

Fast-Scan Cyclic Voltammetry (FSCV) Optimization. Surface characterization illustrates clear topological changes to the GFME surface similar to prior reports using Ar plasma,[13] so plasma treatment power and duration were optimized to produce optimal surfaces for enhanced electrochemical detection of dopamine (DA). The electroanalytical technique FSCV, commonly used for subsecond neurotransmitter fluctuation measurements, was selected as the method of choice for testing the optimizing plasma treatment conditions. As previously stated, Ar plasma treatment does not significantly alter the surface functionality of GFME surfaces, so enhancements to electrochemical detection following treatment can be attributed mostly to increasing surface roughness and defect sites.[13,14,19,26,59] Materials like hydrogenated glassy carbon electrodes report enhanced surface interactions due to high active site density and surface roughness with depleted oxygen functionality;[6,7,55,60] displayed in Raman and XPS analysis, oxygen composition is maintained following Ar plasma treatment permitting strong DA adsorption and reversibility unlike hydrogen plasma treatment. DA detection "optimization" was ultimately quantitated by analyzing electrochemical reversibility. FSCV detection is an adsorption-driven technique where DA redox interactions exhibit fast desorption rates of the oxidized partner, dopamine-o-quinone (DOQ). Because of this, DA does not follow reversible redox interactions at traditional carbon-fiber microelectrodes, with oxidation currents greater than reduction. We hypothesized that plasma treatment conditions would improve electrochemical reversibility, or the ratio of these two currents (ι_{ox}/ι_{red}), due to enhanced surface adsorption interactions and potential local trapping inducing dopamine reversibility.

Fine-tuning Ar plasma treatment was necessary for optimizing the microelectrode's electrochemical performance as low treatment powers/times showed negligible impacts on detection and high treatment powers/times caused microelectrode structural damage. Optimal electrochemical performance was determined by analyzing the Ar plasma treatment conditions that generated the lowest ι_{ox}/ι_{red} value where a value of 1.0 implies a fully reversible redox

interaction. Like CMFEs, untreated GFMEs have an electrochemical reversibility value of ι_{ox}/ι_{red} = ~ 2 (Table 1) showing the need for increased surface roughness to improve redox surface interactions. Untreated and Ar-treated GFMEs were tested electrochemically using the DA FSCV waveform (see Methods) and 1 μM DA, and their electrochemical performance was analyzed (Figure 6). Ar plasma flow rate was maintained at 100 sccm throughout all treatments while the treatment power and time were varied. First, plasma duration was maintained at 60 s while the plasma power was applied in a range of 50 – 150 W. Once an optimal power was determined the flow rate and power were held constant and the treatment duration was applied in a range of 30 – 150 s. Similarly, for both conditions, low treatment times (< 45 s) and powers (< 80 W) fail to adequately roughen the surface providing no electrochemical performance enhancements. Likewise, high treatment times (> 120 s) and powers (> 125 W) cause structural damage to GFMEs rendering inadequate electrochemical detection with instability and decreased signal-to-noise.

Analysis of Ar plasma treatment powers between 90 – 110 W exhibit enhanced DA electrochemical reversibility approaching nearly full reversibility at optimal conditions with minimal changes in nonfaradaic current (Figure 6). For comparison, untreated GFMEs generate an ι_{ox}/ι_{red} value of 1.92 ± 0.14 (n = 6). Here, we show that maintaining a treatment duration of 60 s, while varying plasma power, generates fluctuations in electrochemical reversibility (Figure 6B). 90 W Ar plasma generates no significant change (1.69 ± 0.09, one-way ANOVA, p = 0.1976, n = 6) whereas both 100 W (optimal) and 110 W Ar plasma significantly improve ι_{ox}/ι_{red} to 1.27 ± 0.05*** and 1.50 ± 0.03**, respectively (one-way ANOVA, p = 0.0001 and p = 0.0085, n = 6). We then maintained a plasma treatment of 100 sccm 100 W and varied the application time. Following electrochemical reversibility analysis, we determined 60 s treatment time to be optimal at a Ar plasma flow rate of 100 sccm and power of 100 W (Table 1); optimally Ar treated GFMEs also outperformed all other GFMEs using chemical additives (Figure S1) in terms of electrochemical

reversibility improvements while being much more reproducible (Figure S4). When analyzed using amperometry, optimal Ar plasma treated GFMEs increase the total charge at the electrode's surface by ~ 2-fold (Figure S5, unpaired t-test, $p = 0.0058$, $n = 3$). Optimal treatment conditions create nearly reversible DA redox interactions, and for this reason the surface characterization discussed earlier in this work was performed only on untreated and 60 s 100 W Ar-treated GFMEs. Additionally, our results show no significant increase in non-faradaic current (Figure 6C / Table 2, unpaired t-test, $p = 0.2171$, $n = 6$) while increasing electron transfer kinetics when analyzing the difference in oxidation and reduction peak potentials (ΔE_p, Figure 6D / Table 2, one way ANOVA, $p = 0.0161$, $n = 6$). FSCV characterization of optimally Ar treated GFMEs demonstrate the advantages of their utility for DA detection over untreated GFMEs evident in their enhanced surface morphology for improved DA interfacial interactions.

DA interacts very well at carbon surfaces making it an ideal control analyte for FSCV materials, but many neurochemicals do not interact as favorably. Neurochemicals like serotonin are known to polymerize and foul the electrode's surface depleting surface adsorption sites and hindering detection.[25,61,62] Prior reports provide evidence that GFMEs have innate fouling resistance characteristics,[17,30] so we hypothesized that Ar plasma would not impact these attractive properties due to its inert nature. By applying 25 consecutive injections of 1 μM serotonin, we observe no appreciable change in oxidation current from the 1st to the 25th injection (Figure S6, unpaired t-test, $p = 0.02332$, $n = 6$) implying maintained fouling resistance making them attractive for future *in vivo* studies.

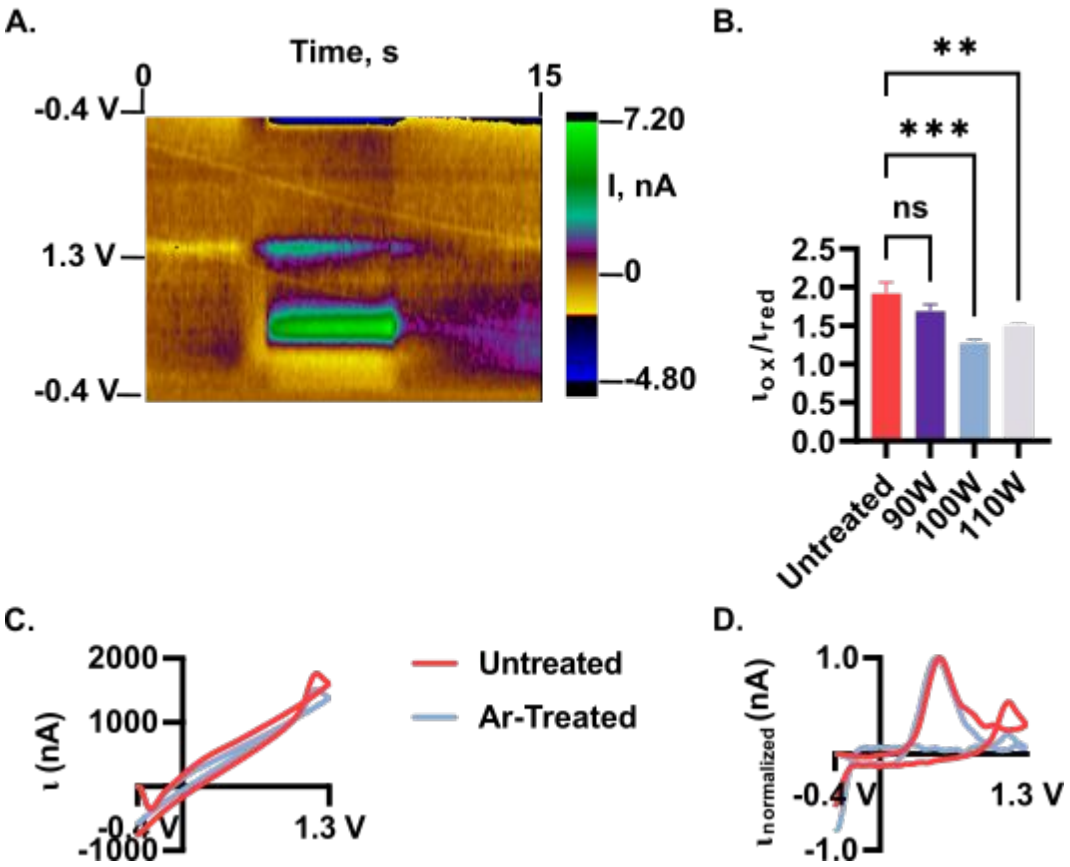

Figure 6. Ar-treated GFMEs exhibit enhanced electrochemical reversibility of dopamine attributed to increased surface roughness improving analyte-electrode interactions with potential for analyte local trapping at roughened sites when analyzed with FSCV. Electrochemical reversibility was optimized using 60 s 100 W Ar plasma for optimized surface roughness. (A) Example false color plot of 1 μM DA detected at 60 s 100 W Ar-treated GO. (B) Optimization of Ar plasma treatment with an electrochemical reversibility of 1.27 ± 0.05 using 100 W power (one-way ANOVA, p = 0.0001, n = 6). (C) Overlayed background current CV of untreated GFMEs (red) and 100 W Ar-treated GFMEs (blue). (D) Overlayed background subtracted CV of untreated GFMEs (red) and 100 W Ar-treated GFMEs (blue).

Table 1. Treatment conditions for optimal Ar plasma treatment with accompanying roughness depth, electrochemical reversibility, and total charge enhancements.

Ar Plasma Power (W)	Roughness height R_z (nm)	I_D/I_G	Electrochemical Reversibility (ι_{ox}/ι_{red})	Q_{total} (nC)
-------	15.2 ± 1.0	1.618 ± 0.005	1.92 ± 0.14	2.82 ± 0.26
90	-------	-------	[c]1.69 ± 0.09[ns]	-------
100	[a]33.4 ± 2.3****	[b]1.857 ± 0.003****	[d]1.27 ± 0.05***	[f]5.45 ± 0.70**
110	-------	-------	[e]1.50 ± 0.03**	-------

[a]Significant increase in surface roughness following 100 W Ar plasma treatment of GO (unpaired t-test, $p < 0.0001$, n = 4). [b]Significant increase in I_D/I_G from untreated to 100 W Ar-treated GO (unpaired t-test, $p < 0.0001$, df = 3451). [c]No significant improvement in dopamine reversibility following 90 W Ar plasma treatment (one-way ANOVA, p = 0.1976, n = 6). [d]Significant

improvement in dopamine reversibility following optimal 100 W Ar plasma treatment (one-way ANOVA, $p = 0.0001$, $n = 6$). [e]Significant improvement in dopamine reversibility following 110 W Ar plasma treatment (one-way ANOVA, $p = 0.0085$, $n = 6$). [f]Significant increase in the total charge generated by the ferri/ferro redox couple at 100 W Ar plasma treated GO (unpaired t-test, $p = 0.0058$, $n = 3$).

Detection Sensitivity and Frequency Dependence. Detection sensitivity and frequency dependence were analyzed to broaden our understanding of DA interactions at untreated and Ar-treated GFMEs. Increasing GFME surface defects and roughness enhance electrochemical reversibility, electron transfer kinetics, and detection sensitivity. DA sensitivity improves from 6.5 $\pm$ 0.3 nA/μM ($R^2 = 0.9418$, $n = 6$) for untreated GFMEs to 11.3 $\pm$ 0.5 nA/μM (Figure 7 / Table 2, $R^2 = 0.9315$, $n = 6$) for optimally Ar-treated GFMEs. By maintaining microfiber diameter, the near 2-fold improvement in DA detection sensitivity is attributed to increased adsorption sites produced by enhanced surface defects increasing edge-plane surface area.[6,7] Untreated GFMEs, according to prior reports,[17,30] possess much lower detection sensitivity to DA providing evidence that future work performed with these surface roughened disk GFMEs could improve spatially-resolved neurochemical detection *in vivo*. Additionally, Ar-treated GFMEs detection sensitivities approach, or surpass, that of traditional CFMEs[1,2,4,13,21] while containing more attractive surface chemistry for DA adsorption interactions.[6,7] Although these results are improved from prior reports,[17,30] there is no statistical change in DA limit of detection for untreated and optimally Ar-treated GMFEs, reduced from 27.9 $\pm$ 4.8 nM to 20.1 $\pm$ 4.5 nM, respectfully (Figure 7 / Table 2, Unpaired t-test, $p = 0.2595$, $n = 6$). Overall, surface roughened GFME's electrochemical performance poses high detection sensitivity capable of improving future DA detection investigations in tissue with FSCV.

FSCV detection is dictated by DA adsorption interactions with carbon surfaces, and, although FSCV is known as a fast detection technique, adsorption hinders measurement temporal resolution. Traditional DA voltammetric sweeps operate at an application frequency of 10 Hz to adequately adsorb DA to the surface causing many rapid events to go unanalyzed. Fortunately, the introduction of carbon nanomaterials has improved frequency independent behavior. These

novel nanomaterials improve temporal resolution permitting the use of higher application frequencies reducing the number of unanalyzed events.[18,22,63] This phenomenon is rooted in attractive crevice/pore geometries on the electrode's surface momentarily trapping and cycling DA's redox species like a thin layer cell environment. [14,18,22,63] The cycling process increases electron transfer rates while limiting diffusional rates improving electrochemical reversibility for frequency independent behavior and temporal resolutions as low as 10 ms. The innate properties of GFMEs provide improved frequency independence[17,30] compared to unmodified CFMEs,[17,63] and our lab has shown further improvements through GO nanosheet orientation.[30] Previously, we developed a modified hydrothermal synthesis process in which we used fluid flow dynamics to orient the edge plane of all GO nanosheets in the direction of the GO microfiber's sensing interface.[30] By aligning the edge plane of GO nanosheets to the electrode's sensing interface, GFMEs become fully frequency independent at an application frequency of 100 Hz unlike the randomly assort GO nanosheets of misaligned GFMEs. The misaligned nanosheet orientation of untreated GFMEs create a 40.3 $\pm$ 10.2% DA oxidation current loss at 100 Hz as compared to 10 Hz (Figure 8 / Table 2, n = 6) similar to prior reports.[17] Our optimally surface roughened GFMEs, however, possess two key qualities known to decrease frequency dependence: surface crevices and defect density similar to edge plane aligned GFMEs. By enhancing the surface roughness and average I_D/I_G (see Raman spectroscopy section) we show true frequency independent behavior in which oxidation current increases 24.6 $\pm$ 17.3% at an application frequency of 100 Hz (Figure 8 / Table 2, unpaired t-test, p = 0.0091, n = 6). Ar-treated GFMEs have an additive effect on frequency independence as deeper crevices accompany greater defect density increasing signal current overtime as application frequency increases and DA is trapped at the surface. Overall, we believe these two microstructure properties allow improved adsorption interactions, momentary trapping, and current amplification of DA otherwise impossible at GFMEs supporting the attractiveness of GO microelectrodes for future FSCV analysis.

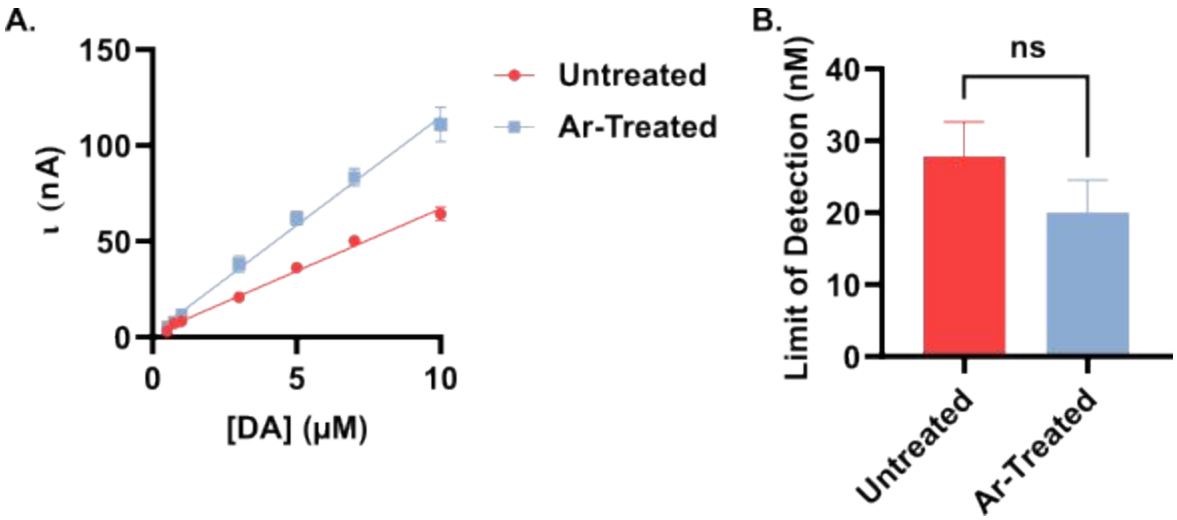

Figure 7. Ar-treated GFMEs (blue) exhibit improved detection sensitivity to dopamine with a lower limit of detection compared to untreated GFMEs (red, n = 6). (A) Concentration curve spanning the linear detection range of dopamine from 0.50 – 10 μM illustrates improved detection sensitivity from 6.5 ± 0.3 nA/μM (R^2 = 0.9418) for untreated GO to 11.3 ± 0.5 nA/μM (R^2 = 0.9315) for Ar-treated GO. (B) Limit of detection reduces from 27.9 ± 4.8 nM for untreated GO to 20.1 ± 4.5 nM (Unpaired t-test, p = 0.2595, n = 6).

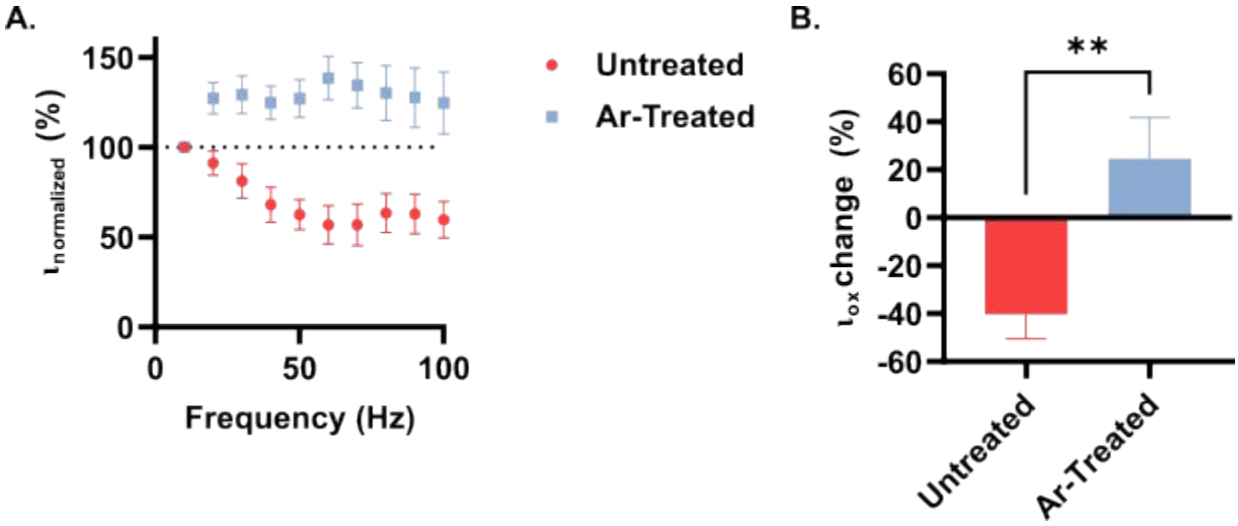

Figure 8. Scan repetition frequency increases show depleted redox interactions of dopamine at untreated GFMEs (red) while Ar-treated GFMEs (blue) illustrate frequency-independent behavior with improved redox reversibility interactions at the electrode interface. (A) Normalized peak oxidation current analysis of 1 μM dopamine at untreated and Ar-treated GFMEs at increasing application frequency. (B) Frequency independence analysis denoted by percent normalized peak oxidation current gained/depleted at the scan repetition frequency of 100 Hz compared to 10 Hz for untreated (40.3 ± 10.2% lost, n = 6) and Ar-treated GFMEs (24.6 ± 17.3% gained, unpaired t-test, p = 0.0091, n = 6).

Table 2. Electrochemical characterization summary of the sensitivity, limit of detection, electron transfer kinetics, capacitive current, electrochemical reversibility ratio, and frequency dependence of untreated and optimally Ar-treated GFMEs.

	ι_{ox}/ι_{red}	ι_c (nA)	ΔE_p (V)	Sensitivity (nA μM^{-1})	Limit of Detection (nM)	ι_{ox} change (+/- %)
Untreated	1.92 ± 0.14	3130 ± 320	0.922 ± 0.024	6.5 ± 0.3	27.9 ± 4.8	-40.3 ± 10.2
Ar-treated	[a]1.27 ± 0.05***	[b]3690 ± 290^{ns}	[c]0.860 ± 0.006*	11.3 ± 0.5	[d]20.1 ± 4.5^{ns}	[e]$+24.6 \pm 17.3$**

[a]Significant improvement in electrochemical reversibility of oxidation-to-reduction current from untreated to optimally Ar-treated GFMEs (one way ANOVA, p = 0.0001, n = 6). [b]No significant change in capacitive current before and after Ar plasma treatment of GFMEs (unpaired t-test, p = 0.2171, n = 6). [c]Significant improvement in electron transfer kinetics comparing untreated and optimally Ar-treated GFMEs (one way ANOVA, p = 0.0161, n = 6). [d]No significant decrease in limit of detect of untreated and Ar-treated GFMEs (unpaired t-test, p = 0.2595, n = 6). [e]Significant change in the oxidation current fluctuation from 10 to 100 Hz application frequency comparing untreated and optimally Ar-treated GFMEs (unpaired t-test, p = 0.0091, n = 6).

Conclusion

In this work, we present an optimized Ar plasma treatment method for fabricating surface roughened, disk GO microelectrodes with excellent electrochemical properties for improved dopamine detection with FSCV. Traditional FSCV detection is performed at amorphous, cylindrical carbon fiber microelectrodes with poorly defined surface chemistry/geometry inadequate for highly temporally resolved measurements. Through various surface characterization techniques, we provide an optimal Ar plasma treatment (100 sccm 60 s 100W) of GO microelectrodes with enhanced surface roughness, defect dense surface chemistry, and unaltered overall chemical functionality. The combination of these surface enhancements and the key properties of GO produce electrode surfaces with improved electron transfer rates and electrochemical reversibility while maintaining fouling resistance. Additionally, optimally treated GFMEs improve dopamine detection sensitivity roughly 2-fold while added surface roughness and defect sites permit frequency independent behavior with increases in oxidation current as

application frequency is increased. Overall, we present a GO microelectrode capable of enhancing FSCV temporal resolution further illustrating the utility of GO microelectrodes and open the door to temporally resolved measurements without the presence of surface porosity or nanosheet alignment.

Supporting Information

We provide additional surface characterization and experiments to support the claims of this manuscript. The supporting information includes SEM imaging of GO microfibers synthesized by non-optimal surface roughening procedures and AFM images of horizontal cross-sections included to illustrate surface roughness quantification. Raman peak fitting analysis was included for both untreated and optimally Ar-treated GFMEs. Lastly, chronoamperometric total charge analysis and a serotonin fouling experiment were included, too.

Conflicts of Interest

The authors declare no conflicts of interest.

Acknowledgements

The research reported here was supported by the National Science Foundation under Award Number 2143520, the National Institute of Allergy and Infectious Diseases of the National Institutes of Health under Award Number R01AI151552, and the Alfred P. Sloan Foundation. The content is solely the responsibility of the authors and does not necessarily reflect the official views of the NSF, NIH, or Alfred P. Sloan Foundation. The authors would also like to thank Dr. Sameera Perera at Wayne State University for acquiring XPS spectra.

References

(1) Bath, B. D.; Michael, D. J.; Trafton, B. J.; Joseph, J. D.; Runnels, P. L.; Wightman, R. M. Subsecond Adsorption and Desorption of Dopamine at Carbon-Fiber Microelectrodes. *Anal. Chem.* **2000**, *72* (24), 5994–6002. https://doi.org/10.1021/ac000849y.
(2) Huffman, M. L.; Venton, B. J. Carbon-Fiber Microelectrodes for in Vivo Applications. *Analyst* **2008**, *134* (1), 18–24. https://doi.org/10.1039/B807563H.
(3) Venton, B. J.; Cao, Q. Fundamentals of Fast-Scan Cyclic Voltammetry for Dopamine Detection. *Analyst* **2020**, *145* (4), 1158–1168. https://doi.org/10.1039/C9AN01586H.

(4) Heien, M. L. A. V.; Phillips, P. E. M.; Stuber, G. D.; Seipel, A. T.; Wightman, R. M. Overoxidation of Carbon-Fiber Microelectrodes Enhances Dopamine Adsorption and Increases Sensitivity. *Analyst* **2003**, *128* (12), 1413–1419. https://doi.org/10.1039/B307024G.
(5) Bucher, E. S.; Wightman, R. M. Electrochemical Analysis of Neurotransmitters. *Annual Review of Analytical Chemistry* **2015**, *8* (1), 239–261. https://doi.org/10.1146/annurev-anchem-071114-040426.
(6) McDermott, M. T.; Kneten, K.; McCreery, R. L. Anthraquinonedisulfonate Adsorption, Electron-Transfer Kinetics, and Capacitance on Ordered Graphite Electrodes: The Important Role of Surface Defects. *J. Phys. Chem.* **1992**, *96* (7), 3124–3130. https://doi.org/10.1021/j100186a063.
(7) McCreery, R. L. Advanced Carbon Electrode Materials for Molecular Electrochemistry. *Chem. Rev.* **2008**, *108* (7), 2646–2687. https://doi.org/10.1021/cr068076m.
(8) Hu, W.; Xiang, R.; Zhang, K.; Xu, Q.; Liu, Y.; Jing, Y.; Zhang, J.; Hu, X.; Zheng, Y.; Jin, Y.; Yang, X.; Lu, C. Electrochemical Performance of Coaxially Wet-Spun Hierarchically Porous Lignin-Based Carbon/Graphene Fiber Electrodes for Flexible Supercapacitors. *ACS Appl. Energy Mater.* **2021**, *4* (9), 9077–9089. https://doi.org/10.1021/acsaem.1c01379.
(9) Chien, A.-T.; Liu, H. C.; Newcomb, B. A.; Xiang, C.; Tour, J. M.; Kumar, S. Polyacrylonitrile Fibers Containing Graphene Oxide Nanoribbons. *ACS Appl. Mater. Interfaces* **2015**, *7* (9), 5281–5288. https://doi.org/10.1021/am508594p.
(10) Gao, Z.; Zhu, J.; Rajabpour, S.; Joshi, K.; Kowalik, M.; Croom, B.; Schwab, Y.; Zhang, L.; Bumgardner, C.; Brown, K. R.; Burden, D.; Klett, J. W.; Duin, A. C. T. van; Zhigilei, L. V.; Li, X. Graphene Reinforced Carbon Fibers. *Science Advances* **2020**, *6* (17), eaaz4191. https://doi.org/10.1126/sciadv.aaz4191.
(11) Cao, Q.; Puthongkham, P.; Venton, B. J. Review: New Insights into Optimizing Chemical and 3D Surface Structures of Carbon Electrodes for Neurotransmitter Detection. *Anal Methods* **2019**, *11* (3), 247–261. https://doi.org/10.1039/C8AY02472C.
(12) Rafi, H.; Zestos, A. G. Review—Recent Advances in FSCV Detection of Neurochemicals via Waveform and Carbon Microelectrode Modification. *J. Electrochem. Soc.* **2021**, *168* (5), 057520. https://doi.org/10.1149/1945-7111/ac0064.
(13) Syeed, A. J.; Li, Y.; Ostertag, B. J.; Brown, J. W.; Ross, A. E. Nanostructured Carbon-Fiber Surfaces for Improved Neurochemical Detection. *Faraday Discuss.* **2021**. https://doi.org/10.1039/D1FD00049G.
(14) Ostertag, B.; Ross, A. E. Wet-Spun Porous Carbon Microfibers for Enhanced Electrochemical Detection. *ACS Appl. Mater. Interfaces* **2023**, *15* (14), 17601–17611. https://doi.org/10.1021/acsami.3c00423.
(15) Li, Y.; Keller, A. L.; Cryan, M. T.; Ross, A. E. Metal Nanoparticle Modified Carbon-Fiber Microelectrodes Enhance Adenosine Triphosphate Surface Interactions with Fast-Scan Cyclic Voltammetry. *ACS Meas. Sci. Au* **2022**, *2* (2), 96–105. https://doi.org/10.1021/acsmeasuresciau.1c00026.
(16) Keller, A. L.; Quarin, S. M.; Strobbia, P.; Ross, A. E. Platinum Nanoparticle Size and Density Impacts Purine Electrochemistry with Fast-Scan Cyclic Voltammetry. *J. Electrochem. Soc.* **2022**, *169* (4), 046514. https://doi.org/10.1149/1945-7111/ac65bc.
(17) Li, Y.; Jarosova, R.; Weese-Myers, M. E.; Ross, A. E. Graphene-Fiber Microelectrodes for Ultrasensitive Neurochemical Detection. *Anal. Chem.* **2022**, *94* (11), 4803–4812. https://doi.org/10.1021/acs.analchem.1c05637.
(18) Yang, C.; Hu, K.; Wang, D.; Zubi, Y.; Lee, S. T.; Puthongkham, P.; Mirkin, M. V.; Venton, B. J. Cavity Carbon-Nanopipette Electrodes for Dopamine Detection. *Anal. Chem.* **2019**, *91* (7), 4618–4624. https://doi.org/10.1021/acs.analchem.8b05885.
(19) Cao, Q.; Hensley, D. K.; Lavrik, N. V.; Venton, B. J. Carbon Nanospikes Have Better Electrochemical Properties than Carbon Nanotubes Due to Greater Surface Roughness and Defect Sites. *Carbon* **2019**, *155*, 250–257. https://doi.org/10.1016/j.carbon.2019.08.064.

(20) Chang, Y.; Venton, B. J. Optimization of Graphene Oxide-Modified Carbon-Fiber Microelectrode for Dopamine Detection. *Anal Methods* **2020**, *12* (22), 2893–2902. https://doi.org/10.1039/d0ay00310g.
(21) Ostertag, B. J.; Cryan, M. T.; Serrano, J. M.; Liu, G.; Ross, A. E. Porous Carbon Nanofiber-Modified Carbon Fiber Microelectrodes for Dopamine Detection. *ACS Appl. Nano Mater.* **2022**, *5* (2), 2241–2249. https://doi.org/10.1021/acsanm.1c03933.
(22) Shao, Z.; Puthongkham, P.; Hu, K.; Jia, R.; Mirkin, M. V.; Venton, B. J. Thin Layer Cell Behavior of CNT Yarn and Cavity Carbon Nanopipette Electrodes: Effect on Catecholamine Detection. *Electrochimica Acta* **2020**, *361*, 137032. https://doi.org/10.1016/j.electacta.2020.137032.
(23) Mendoza, A.; Asrat, T.; Liu, F.; Wonnenberg, P.; Zestos, A. G. Carbon Nanotube Yarn Microelectrodes Promote High Temporal Measurements of Serotonin Using Fast Scan Cyclic Voltammetry. *Sensors (Basel)* **2020**, *20* (4), 1173. https://doi.org/10.3390/s20041173.
(24) Schmidt, A. C.; Wang, X.; Zhu, Y.; Sombers, L. A. Carbon Nanotube Yarn Electrodes for Enhanced Detection of Neurotransmitter Dynamics in Live Brain Tissue. *ACS Nano* **2013**, *7* (9), 7864–7873. https://doi.org/10.1021/nn402857u.
(25) Hashemi, P.; Dankoski, E. C.; Petrovic, J.; Keithley, R. B.; Wightman, R. M. Voltammetric Detection of 5-Hydroxytryptamine Release in the Rat Brain. *Anal Chem* **2009**, *81* (22), 9462–9471. https://doi.org/10.1021/ac9018846.
(26) Puthongkham, P.; Yang, C.; Venton, B. J. Carbon Nanohorn-Modified Carbon Fiber Microelectrodes for Dopamine Detection. *Electroanalysis* **2018**, *30* (6), 1073–1081. https://doi.org/10.1002/elan.201700667.
(27) Zestos, A. G.; Yang, C.; Jacobs, C. B.; Hensley, D.; Venton, B. J. Carbon Nanospikes Grown on Metal Wires as Microelectrode Sensors for Dopamine. *Analyst* **2015**, *140* (21), 7283–7292. https://doi.org/10.1039/C5AN01467K.
(28) Ambrosi, A.; Chua, C. K.; Bonanni, A.; Pumera, M. Electrochemistry of Graphene and Related Materials. *Chem. Rev.* **2014**, *114* (14), 7150–7188. https://doi.org/10.1021/cr500023c.
(29) Kuila, T.; Bose, S.; Khanra, P.; Mishra, A. K.; Kim, N. H.; Lee, J. H. Recent Advances in Graphene-Based Biosensors. *Biosensors and Bioelectronics* **2011**, *26* (12), 4637–4648. https://doi.org/10.1016/j.bios.2011.05.039.
(30) Jarosova, R.; J. Ostertag, B.; E. Ross, A. Graphene Oxide Fiber Microelectrodes with Controlled Sheet Alignment for Sensitive Neurotransmitter Detection. *Nanoscale* **2023**. https://doi.org/10.1039/D3NR02879H.
(31) Mkhoyan, K. A.; Contryman, A. W.; Silcox, J.; Stewart, D. A.; Eda, G.; Mattevi, C.; Miller, S.; Chhowalla, M. Atomic and Electronic Structure of Graphene-Oxide. *Nano Lett.* **2009**, *9* (3), 1058–1063. https://doi.org/10.1021/nl8034256.
(32) Wang, S.; Dong, Y.; He, C.; Gao, Y.; Jia, N.; Chen, Z.; Song, W. The Role of Sp2/Sp3 Hybrid Carbon Regulation in the Nonlinear Optical Properties of Graphene Oxide Materials. *RSC Adv.* **2017**, *7* (84), 53643–53652. https://doi.org/10.1039/C7RA10505C.
(33) Li, M.; Zhang, X.; Wang, X.; Ru, Y.; Qiao, J. Ultrastrong Graphene-Based Fibers with Increased Elongation. *Nano Lett.* **2016**, *16* (10), 6511–6515. https://doi.org/10.1021/acs.nanolett.6b03108.
(34) Xu, Y.; Lin, Z.; Zhong, X.; Huang, X.; Weiss, N. O.; Huang, Y.; Duan, X. Holey Graphene Frameworks for Highly Efficient Capacitive Energy Storage. *Nat Commun* **2014**, *5* (1), 1–8. https://doi.org/10.1038/ncomms5554.
(35) He, R.; Cong, S.; Wang, J.; Liu, J.; Zhang, Y. Porous Graphene Oxide/Porous Organic Polymer Hybrid Nanosheets Functionalized Mixed Matrix Membrane for Efficient CO2 Capture. *ACS Appl. Mater. Interfaces* **2019**, *11* (4), 4338–4344. https://doi.org/10.1021/acsami.8b17599.

(36) Kim, J.; Eum, J.-H.; Kang, J.; Kwon, O.; Kim, H.; Kim, D. W. Tuning the Hierarchical Pore Structure of Graphene Oxide through Dual Thermal Activation for High-Performance Supercapacitor. *Sci Rep* **2021**, *11* (1), 2063. https://doi.org/10.1038/s41598-021-81759-7.

(37) Romanos, J.; Beckner, M.; Rash, T.; Firlej, L.; Kuchta, B.; Yu, P.; Suppes, G.; Wexler, C.; Pfeifer, P. Nanospace Engineering of KOH Activated Carbon. *Nanotechnology* **2012**, *23* (1), 015401. https://doi.org/10.1088/0957-4484/23/1/015401.

(38) Zhu, Y.; Murali, S.; Stoller, M. D.; Ganesh, K. J.; Cai, W.; Ferreira, P. J.; Pirkle, A.; Wallace, R. M.; Cychosz, K. A.; Thommes, M.; Su, D.; Stach, E. A.; Ruoff, R. S. Carbon-Based Supercapacitors Produced by Activation of Graphene. *Science* **2011**, *332* (6037), 1537–1541. https://doi.org/10.1126/science.1200770.

(39) Taylor, I. M.; Robbins, E. M.; Catt, K. A.; Cody, P. A.; Weaver, C. L.; Cui, X. T. Enhanced Dopamine Detection Sensitivity by PEDOT/Graphene Oxide Coating on in Vivo Carbon Fiber Electrodes. *Biosens Bioelectron* **2017**, *89* (Pt 1), 400–410. https://doi.org/10.1016/j.bios.2016.05.084.

(40) Cheng, R.; Colombo, R. N. P.; Zhang, L.; Nguyen, D. H. T.; Tilley, R.; Cordoba de Torresi, S. I.; Dai, L.; Gooding, J. J.; Gonçales, V. R. Porous Graphene Oxide Films Prepared via the Breath-Figure Method: A Simple Strategy for Switching Access of Redox Species to an Electrode Surface. *ACS Appl. Mater. Interfaces* **2020**, *12* (49), 55181–55188. https://doi.org/10.1021/acsami.0c16811.

(41) Li, Z.; Xu, Z.; Liu, Y.; Wang, R.; Gao, C. Multifunctional Non-Woven Fabrics of Interfused Graphene Fibres. *Nat Commun* **2016**, *7* (1), 13684. https://doi.org/10.1038/ncomms13684.

(42) Castagnola, E.; Garg, R.; Rastogi, S. K.; Cohen-Karni, T.; Cui, X. T. 3D Fuzzy Graphene Microelectrode Array for Dopamine Sensing at Sub-Cellular Spatial Resolution. *Biosensors and Bioelectronics* **2021**, *191*, 113440. https://doi.org/10.1016/j.bios.2021.113440.

(43) Zheng, X.; Hu, Q.; Zhou, X.; Nie, W.; Li, C.; Yuan, N. Graphene-Based Fibers for the Energy Devices Application: A Comprehensive Review. *Materials & Design* **2021**, *201*, 109476. https://doi.org/10.1016/j.matdes.2021.109476.

(44) Xu, Z.; Sun, H.; Zhao, X.; Gao, C. Ultrastrong Fibers Assembled from Giant Graphene Oxide Sheets. *Advanced Materials* **2013**, *25* (2), 188–193. https://doi.org/10.1002/adma.201203448.

(45) Xin, G.; Zhu, W.; Deng, Y.; Cheng, J.; Zhang, L. T.; Chung, A. J.; De, S.; Lian, J. Microfluidics-Enabled Orientation and Microstructure Control of Macroscopic Graphene Fibres. *Nature Nanotech* **2019**, *14* (2), 168–175. https://doi.org/10.1038/s41565-018-0330-9.

(46) Hofmann, E.; Krüger, K.; Haynl, C.; Scheibel, T.; Trebbin, M.; Förster, S. Microfluidic Nozzle Device for Ultrafine Fiber Solution Blow Spinning with Precise Diameter Control. *Lab Chip* **2018**, *18* (15), 2225–2234. https://doi.org/10.1039/C8LC00304A.

(47) Mao, Y.; Huang, Q.; Meng, B.; Zhou, K.; Liu, G.; Gugliuzza, A.; Drioli, E.; Jin, W. Roughness-Enhanced Hydrophobic Graphene Oxide Membrane for Water Desalination via Membrane Distillation. *Journal of Membrane Science* **2020**, *611*, 118364. https://doi.org/10.1016/j.memsci.2020.118364.

(48) Li, J.; Li, J.; Li, L.; Yu, M.; Ma, H.; Zhang, B. Flexible Graphene Fibers Prepared by Chemical Reduction-Induced Self-Assembly. *J. Mater. Chem. A* **2014**, *2* (18), 6359–6362. https://doi.org/10.1039/C4TA00431K.

(49) Gao, J.; Liu, F.; Liu, Y.; Ma, N.; Wang, Z.; Zhang, X. Environment-Friendly Method To Produce Graphene That Employs Vitamin C and Amino Acid. *Chem. Mater.* **2010**, *22* (7), 2213–2218. https://doi.org/10.1021/cm902635j.

(50) Ferrari, A. C.; Basko, D. M. Raman Spectroscopy as a Versatile Tool for Studying the Properties of Graphene. *Nature Nanotech* **2013**, *8* (4), 235–246. https://doi.org/10.1038/nnano.2013.46.

(51) Ferrari, A. C.; Robertson, J. Interpretation of Raman Spectra of Disordered and Amorphous Carbon. *Phys. Rev. B* **2000**, *61* (20), 14095–14107. https://doi.org/10.1103/PhysRevB.61.14095.
(52) King, A. A. K.; Davies, B. R.; Noorbehesht, N.; Newman, P.; Church, T. L.; Harris, A. T.; Razal, J. M.; Minett, A. I. A New Raman Metric for the Characterisation of Graphene Oxide and Its Derivatives. *Sci Rep* **2016**, *6* (1), 19491. https://doi.org/10.1038/srep19491.
(53) Claramunt, S.; Varea, A.; López-Díaz, D.; Velázquez, M. M.; Cornet, A.; Cirera, A. The Importance of Interbands on the Interpretation of the Raman Spectrum of Graphene Oxide. *J. Phys. Chem. C* **2015**, *119* (18), 10123–10129. https://doi.org/10.1021/acs.jpcc.5b01590.
(54) Jung, W. T.; Jang, H.-S.; Jeon, J. W.; Kim, B. H. Effect of Oxygen Functional Groups in Reduced Graphene Oxide-Coated Silk Electronic Textiles for Enhancement of NO2 Gas-Sensing Performance. *ACS Omega* **2021**, *6* (41), 27080–27088. https://doi.org/10.1021/acsomega.1c03658.
(55) Chen, Q.; Swain, G. M. Structural Characterization, Electrochemical Reactivity, and Response Stability of Hydrogenated Glassy Carbon Electrodes. *Langmuir* **1998**, *14* (24), 7017–7026. https://doi.org/10.1021/la980907z.
(56) Li, Y.; Ross, A. E. Plasma-Treated Carbon-Fiber Microelectrodes for Improved Purine Detection with Fast-Scan Cyclic Voltammetry. *Analyst* **2020**, *145* (3), 805–815. https://doi.org/10.1039/C9AN01636H.
(57) Tashima, D.; Sakamoto, A.; Taniguchi, M.; Sakoda, T.; Otsubo, M. Surface Modification of Carbon Electrodes Using an Argon Plasma. *Vacuum* **2008**, *83* (3), 695–698. https://doi.org/10.1016/j.vacuum.2008.04.060.
(58) Ghamouss, F.; Luais, E.; Thobie-Gautier, C.; Tessier, P.-Y.; Boujtita, M. Argon Plasma Treatment to Enhance the Electrochemical Reactivity of Screen-Printed Carbon Surfaces. *Electrochimica Acta* **2009**, *54* (11), 3026–3032. https://doi.org/10.1016/j.electacta.2008.12.011.
(59) Johnson, J. A.; Wightman, R. M. Cyclic Voltammetric Measurements of Neurotransmitters. *Electrochem. Soc. Interface* **2017**, *26* (3), 53. https://doi.org/10.1149/2.F06173if.
(60) Xu, J.; Chen, Q.; Swain, G. M. Anthraquinonedisulfonate Electrochemistry: A Comparison of Glassy Carbon, Hydrogenated Glassy Carbon, Highly Oriented Pyrolytic Graphite, and Diamond Electrodes. *Anal. Chem.* **1998**, *70* (15), 3146–3154. https://doi.org/10.1021/ac9800661.
(61) Abdalla, A.; Atcherley, C. W.; Pathirathna, P.; Samaranayake, S.; Qiang, B.; Peña, E.; Morgan, S. L.; Heien, M. L.; Hashemi, P. In Vivo Ambient Serotonin Measurements at Carbon-Fiber Microelectrodes. *Anal Chem* **2017**, *89* (18), 9703–9711. https://doi.org/10.1021/acs.analchem.7b01257.
(62) Jacobs, C. B.; Peairs, M. J.; Venton, B. J. Review: Carbon Nanotube Based Electrochemical Sensors for Biomolecules. *Analytica Chimica Acta* **2010**, *662* (2), 105–127. https://doi.org/10.1016/j.aca.2010.01.009.
(63) Cao, Q.; Shao, Z.; Hensley, D. K.; Lavrik, N. V.; Venton, B. J. Influence of Geometry on Thin Layer and Diffusion Processes at Carbon Electrodes. *Langmuir* **2021**, *37* (8), 2667–2676. https://doi.org/10.1021/acs.langmuir.0c03315.

TOC Graphic

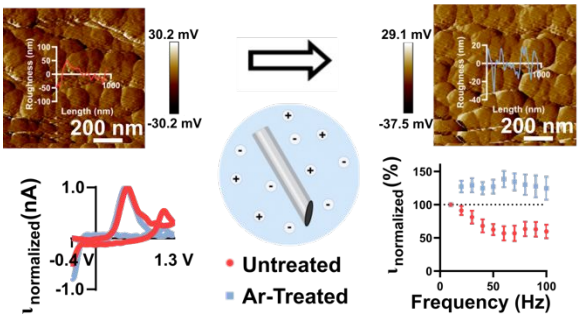
30.2 mV
-30.2 mV
200 nm
Roughness (nm)
Length (nm)
29.1 mV
-37.5 mV
200 nm
1.0
-1.0
-0.4 V
1.3 V
I normalized (nA)
Untreated
Ar-Treated
I normalized (%)
150
100
50
0
0
50
100
Frequency (Hz)